

Measuring BAO and non-Gaussianity via QSO clustering

U. Sawangwit^{1*}, T. Shanks¹, S. M. Croom², M. J. Drinkwater³, S. Fine¹,
D. Parkinson³ & Nicholas P. Ross⁴

¹*Dept. of Physics, Durham University, South Road, Durham, DH1 3LE, UK*

²*Sydney Institute for Astronomy, School of Physics, University of Sydney, NSW 2006, Australia*

³*School of Mathematics & Physics, The University of Queensland, Brisbane QLD 4072, Australia*

⁴*Lawrence Berkeley National Laboratory, One Cyclotron Road, Berkeley, CA 94720, USA*

Accepted 2011 September 16. Received 2011 September 16; in original form 2011 June 5

ABSTRACT

Our goals are (i) to search for BAO and large-scale structure in current QSO survey data and (ii) to use these and simulation/forecast results to assess the science case for a new, $\gtrsim 10\times$ larger, QSO survey. We first combine the SDSS, 2QZ and 2SLAQ surveys to form a survey of ≈ 60000 QSOs. We find a hint of a peak in the QSO 2-point correlation function, $\xi(s)$, at the same scale ($\approx 105h^{-1}\text{Mpc}$) as detected by Eisenstein et al. (2005) in their sample of DR5 LRGs but only at low statistical significance. We then compare these data with QSO mock catalogues from the Hubble Volume N-body light-cone simulation used by Hoyle et al. (2002) and find that both routes give statistical error estimates that are consistent at $\approx 100h^{-1}\text{Mpc}$ scales. Mock catalogues are then used to estimate the nominal survey size needed for a $3-4\sigma$ detection of the BAO peak. We find that a redshift survey of ≈ 250000 $z < 2.2$ QSOs is required over $\approx 3000\text{deg}^2$. This is further confirmed by static log-normal simulations where the BAO are clearly detectable in the QSO power spectrum and correlation function. The nominal survey would on its own produce the first detection of, for example, discontinuous dark energy evolution in the so far uncharted $1 < z < 2.2$ redshift range. *We further find that a survey with $\approx 50\%$ higher QSO sky densities and 50% bigger area will give an $\approx 6\sigma$ BAO detection, leading to an error $\approx 60\%$ of the size of the BOSS error on the dark energy evolution parameter, w_a .*

Another important aim for a QSO survey is to place new limits on primordial non-Gaussianity at large scales. In particular, it is important to test tentative evidence we have found for the evolution of the linear form of the combined SDSS+2QZ+2SLAQ QSO $\xi(s)$ at $z \approx 1.6$, which may be caused by the existence of non-Gaussian clustering features at high redshift. Such a QSO survey will also determine the gravitational growth rate at $z \approx 1.6$ via redshift-space distortions, allow lensing tomography via QSO magnification bias while also measuring the exact luminosity dependence of small-scale QSO clustering.

Key words: quasar clustering

1 INTRODUCTION

Quasi-stellar objects (QSOs) have been used as tracers of large-scale structure for many years now. The first measurements were made by Osmer (1981), then with the arrival of high-multiplex fibre systems, the subject advanced rapidly (e.g. Boyle, Shanks, & Peterson 1988; Croom et al. 2005; da Ângela et al. 2008; Ross et al. 2009 and references therein). Their clustering at small scales as measured by the correlation function is known to be consistent with the usual

$\gamma = -1.8$ power-law form for galaxies. The amplitude is comparable to galaxies at low redshifts and remains reasonably constant with redshift. At larger scales the power spectrum has been measured to be reasonably consistent with the standard ΛCDM cosmological model (e.g. Hoyle et al. 2002; Outram et al. 2003).

Here, we have combined the largest, spectroscopically confirmed, QSO surveys from fibre spectrographs including 2QZ (Croom et al. 2004), 2SLAQ (Croom et al. 2009) and SDSS DR5 (Schneider et al. 2007) to form a redshift survey comprising some ≈ 60000 QSOs. We have already found in these datasets that the small scale clustering of QSOs is

* E-mail: utane.sawangwit@durham.ac.uk (US)

remarkably independent of QSO luminosity at fixed redshift (Shanks et al. 2011).

In this paper, we first use the above combined survey to estimate the large-scale QSO correlation function and search for the BAO feature. We then outline our initial motivation for an extended QSO redshift survey using the ‘effective survey volume’ as a measure of clustering ‘grasp’. We then make an empirical test of the errors on the QSO correlation function at $\approx 100h^{-1}\text{Mpc}$ scales using both the data and mock QSO catalogues from the Hubble Volume N-body simulation. These routes allow a first estimate of the survey size needed for a significant BAO detection. We particularly focus on surveys that could be made with 2dF (Lewis et al. 2002) and AAOmega (Smith et al. 2004) at the AAT (c.f. the results of Wang et al. (2009) for QSO surveys with LAMOST). We then use static log-normal simulations to test further BAO detectability and use Fisher matrix and Markov Chain Monte Carlo (MCMC) methods to test a QSO survey’s competitiveness against other routes to the BAO scale and the evolution of w . Finally, we look at the prospects for detecting evidence for non-Gaussian clustering at large scales via a QSO survey, in particular focussing on the possibility that the current QSO surveys show evidence for evolution in the linear regime of clustering, which might represent evidence for non-Gaussianity, if confirmed in a larger survey.

2 QSO CLUSTERING DATA

We start by making a study of the results from current QSO surveys (a) to see if the BAO peak can be detected in the correlation function and (b) to measure the errors to base an empirical estimate of the new survey size needed for an accurate BAO measurement. This survey size estimate will then be compared to those from simulations to determine the best QSO survey strategy in terms of area and magnitude limit.

2.1 SDSS, 2QZ and 2SLAQ surveys

Previously Croom et al. (2005) used the 2QZ survey to estimate the QSO correlation function and its dependence on redshift and luminosity. This survey contained ≈ 22655 QSOs in two $\approx 375\text{deg}^2$ NGC + SGC strips. The magnitude limit was $18.25 < b_J < 20.85$ and the resulting QSO sky density was 31deg^{-2} . Croom et al. (2005) measured $s_0 = 5.4_{-0.48}^{+0.42}h^{-1}\text{Mpc}$ and $\gamma = 1.2 \pm 0.1$ at $1 < s < 25h^{-1}\text{Mpc}$ for the amplitude and slope of the z -space correlation function, $\xi(s)$.

da Ângela et al. (2008) then used the 2SLAQ survey of 9418 QSOs based on SDSS imaging to test the luminosity dependence of the QSO clustering. The magnitude limit was $20.5 < g_{AB}(\approx b_J) < 21.85$ and the resulting QSO sky density was $\approx 45\text{deg}^{-2}$, including the 2dF QSOs where the two surveys overlapped, in a total area of $\approx 200\text{deg}^2$. da Ângela et al. (2008) found a $\xi(s)$ amplitude and slope similar to that for 2QZ.

Most recently, Ross et al. (2009) have analysed the clustering of 30239 QSOs in the 4013deg^2 SDSS DR5 survey to $i_{AB} = 19.1$. This gives a QSO sky density of 7.5deg^{-2} in the uniform sample where Ross et al. (2009) measured

$s_0 = 5.95 \pm 0.45h^{-1}\text{Mpc}$ and $\gamma = 1.16_{-0.16}^{+0.11}$ in the $1 < s < 25h^{-1}\text{Mpc}$ range.

2.2 Large-scale clustering comparison

Here, the clustering analysis has been re-done to use consistent bins at comoving separations corresponding to BAO scales in the 2QZ, 2SLAQ and SDSS-DR5 spectroscopic QSO samples. The data and random catalogues are the same as those used in the analyses of da Ângela et al. (2008) and Ross et al. (2009) for 2QZ+2SLAQ and SDSS-DR5, respectively. We used the ‘UNIFORM’ sample with $0.3 \leq z \leq 2.2$ of Ross et al. (2009) which contains 30239 QSOs over 4013deg^2 . The 2QZ+2SLAQ sample contains 28790 $0.3 < z < 2.9$ QSOs and its small- and intermediate-scale clustering analyses have been performed by da Ângela et al. (2008) (see also Croom et al. (2005) for the 2QZ-only clustering analysis). We perform a new clustering analysis by counting pairs at separation, s , independently for the SDSS and 2QZ+2SLAQ samples. The data-random, DR , and random-random, RR , pairs for each sample are normalised by N_{rd} and N_{rd}^2 , respectively, where N_{rd} is the ratio between numbers of randoms and data (≈ 20 for the 2QZ+2SLAQ and ≈ 30 for the SDSS samples). The Landy & Szalay (1993) estimator is then used to determine the $\xi(s)$ from the summed pairs over the different samples. Note that the results are in good agreement with those using the Hamilton (1993) estimator.

In Fig. 1 we then compare the large-scale clustering results from the three surveys directly with each other using the redshift-space correlation function, $\xi(s)$. The cosmology assumed in all cases is $\Omega_\Lambda = 0.7$, $\Omega_m = 0.3$. Fitting the $\xi(s)$ results consistently in the $1 < s < 30h^{-1}\text{Mpc}$ range, Shanks et al. (2011) fitted real-space correlation function scale-lengths, r_0 , assuming power-law slope, $\gamma = 1.8$, infall parameter, $\beta = 0.4$, and line-of-sight pairwise velocity dispersion $\langle w^2 \rangle^{1/2} = 750\text{kms}^{-1}$. These authors found agreement at the 1.4σ significance level in these results with SDSS giving $r_0 = 6.30 \pm 0.3h^{-1}\text{Mpc}$, 2QZ giving $r_0 = 5.75 \pm 0.25h^{-1}\text{Mpc}$ and 2SLAQ giving $r_0 = 5.70 \pm 0.35h^{-1}\text{Mpc}$. The best overall fit is $r_0 = 5.90 \pm 0.14h^{-1}\text{Mpc}$. Thus the small-scale results suggest that it is reasonable to combine these 3 surveys and the $\xi(s)$ result at large-scales is also shown in Fig. 1. The data is compared to a LCDM model and a ‘wiggle-free’ version of the model (Eisenstein & Hu 1998). These models are normalised to match the data at $s = 10 - 30h^{-1}\text{Mpc}$ (see Fig. 9 below). The errors are based on Poisson errors calibrated by jack-knife errors in all 3 cases. Generally the SDSS has the biggest errors, particularly at the smaller scales. This is because of its relatively low sky density. This means that at $\approx 100h^{-1}\text{Mpc}$ the 2QZ (and 2SLAQ) surveys dominate the statistics at the predicted BAO scale. The 2QZ survey error is $\approx 2\times$ smaller than the SDSS error and $1.8\times$ smaller than the 2SLAQ error. The blue filled circles then represent the overall 2QZ+2SLAQ+SDSS result, produced by simply adding the QSO-QSO and QSO-random pairs across the surveys. The resulting error is $\approx 2\times$ larger than the error from the SDSS LRG sample of Eisenstein et al. (2005). We see that there is some hint of a detection at $105h^{-1}\text{Mpc}$ but there is a similarly sized feature at $\approx 85h^{-1}\text{Mpc}$. Clearly while the data appear promising in terms of detecting the BAO

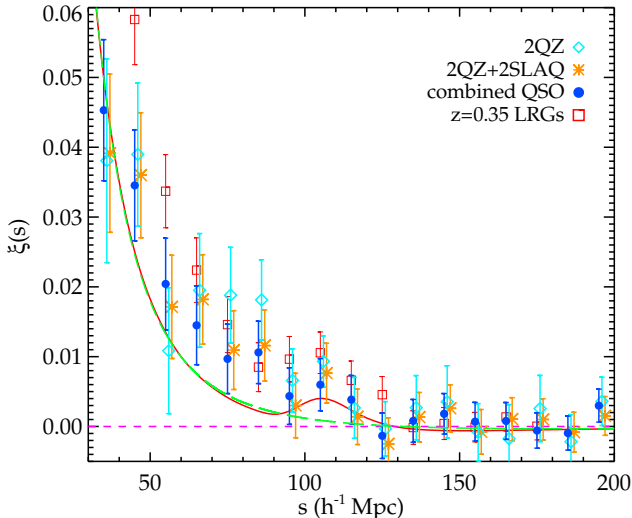


Figure 1. The large-scale redshift-space correlation function results from the 2QZ, the 2QZ+2SLAQ and the combined SDSS DR5+2QZ+2SLAQ QSO surveys. The errors are empirically scaled by the average ($1.2\times$) ratio of jack-knife to Poisson errors in this separation range. The results are compared to Λ CDM (red solid) and no-wiggle (green dashed) models and also the $z = 0.35$ LRG result of Eisenstein et al. (2005).

feature, a larger sample size is needed and in Section 5 below we will translate these empirical errors into a required survey size to measure the BAO scale. We shall also compare with the errors predicted by simulations and use these to optimise the properties of a new QSO redshift survey for large-scale clustering.

3 QSO SURVEY EFFECTIVE VOLUME

We next estimate the efficiency of future QSO clustering surveys via their effective volume (V_{eff}). Although QSO sky densities are lower than for galaxy surveys, their clustering amplitude is relatively high, the exposure time required to establish redshifts is generally quite short, contamination rates are increasingly low and the volumes probed are very large. Moreover, the low QSO sky density can be viewed as an advantage in that it may well match the fibre density currently available from instruments like AAT 2dF.

A rough measure of a survey’s capability for power spectrum or 2-point correlation function analysis, the effective volume is defined by Eisenstein et al. (2005) and represents the survey volume that has a high enough QSO density for the shot noise to lie below the amplitude of a spatial power spectrum feature such as a BAO oscillation scale. The power spectrum or correlation function error at a particular scale then is proportional to $V_{eff}^{-1/2}$. In Fig. 2 we have calculated the effective volume for QSO surveys assuming the SDSS DR5 QSO $n(z)$ in the redshift range $0.5 < z < 2.2$ (see also Fig. 2 of Wang et al. 2009). We have chosen a nominal survey area of 3000deg^2 ; effective volumes of other survey areas will scale linearly. Since the QSO $n(z)$ is approximately independent of survey magnitude limit, the main other survey parameter is QSO sky density. We have cal-

culated the effective volume at sky densities approximating those for the SDSS, 2QZ and 2SLAQ surveys at 10, 35 and 80deg^{-2} . We also present the effective volumes at 140deg^{-2} , which is approximately the largest density accommodated by the 2dF fibre positioner (if tiling overlaps is considered, see later), and 280deg^{-2} which is the highest QSO density that is available from the Hubble Volume simulations (see Sect. 4.1). The assumed QSO correlation function amplitude was $s_0 = 6h^{-1}\text{Mpc}$ which is also found to be almost independent of survey limit (see eg Shanks et al. 2011). From Fig. 2 we see that QSO effective volume generally drops sharply as the spatial wavenumber increases; this drop is at a faster rate than for more highly sampled galaxy surveys such as WiggleZ.

However, even at the 2SLAQ sky density of 80deg^{-2} , we see that at the scale of the first acoustic peak at $k \approx 0.02h\text{Mpc}^{-1}$, the effective volume of our nominal 3000deg^2 survey overtakes that of the current leading galaxy BAO survey, WiggleZ (Blake et al. 2011), by a factor of ≈ 3 . Of course, even if the effective volume is only merely competitive with WiggleZ volume as it is at the 2nd and 3rd peak positions, then this still represents an advance, given the $\approx 3\times$ higher redshifts of the QSOs than the WiggleZ galaxies. To reach the same effective volume at the first acoustic peak of the current BOSS LRG survey at $z \approx 0.55$, a higher QSO sky density of 140deg^{-2} would be needed. This sky density would be reached at $g \approx 22.7^1$, assuming a $10^{0.3m}$ QSO number count slope (Boyle, Shanks, & Peterson 1988). This QSO effective volume again applies at an $\approx 3\times$ higher redshift than the BOSS LRGs. Even the BigBOSS ELG survey will produce an effective volume which is only $\approx 2\times$ bigger than for a 140deg^{-2} QSO survey when renormalised to the same area of sky. BigBOSS also has a significantly lower average redshift, $z \approx 1$. Thus the relatively crude effective volume measure suggests that a QSO survey of nominal area 3000deg^2 and sky density in the range $80\text{--}140\text{deg}^{-2}$ should produce large-scale clustering results that have similar precision at the first acoustic peak to the BOSS LRG survey but at significantly higher redshift.

4 BAO SEARCH IN SIMULATIONS

4.1 Hubble Volume

We next use the Hubble Volume simulation to measure the correlation function errors directly in mock surveys that range up to higher QSO sky densities than 2QZ. This simulation (Evvard et al. 2002) used an initial mass power spectrum with $\Omega_b = 0.04$, $\Omega_{\text{CDM}} = 0.26$, $\Omega_\Lambda = 0.7$, $H_0 = 70\text{ km s}^{-1}\text{ Mpc}^{-1}$ and $\sigma_8 = 0.9$. Mock QSO catalogues from this simulation were generated by Hoyle et al. (2002). We did consider using newer simulations but although these frequently had higher resolution, they generally did not have sufficient volume to accommodate even the original 2QZ survey. The Hubble Volume mocks are made in the form of past light cones as needed for accurate modelling of the QSO survey. The mock QSOs bias relative to the mass was modelled according to the algorithm of Hatton & Cole (1998).

¹ We assume that the QSO clustering and bias continue to be luminosity independent at this limit (Shanks et al. 2011).

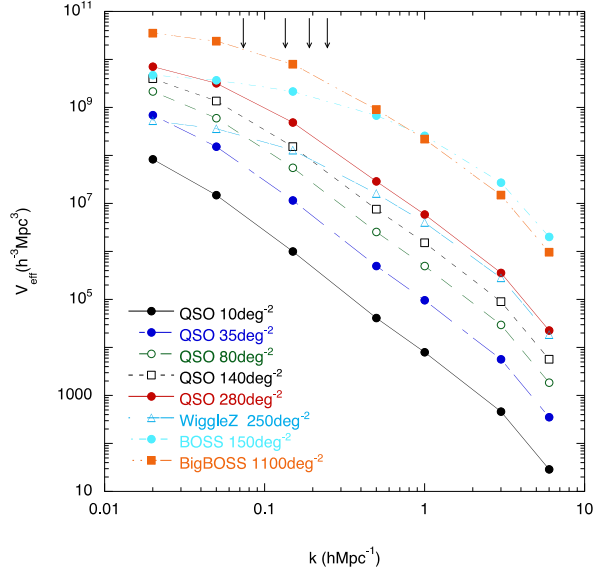


Figure 2. The effective volume as a function of wavenumber of spatial scale for a $z \approx 1.5$ QSO survey of area 3000deg^2 and QSO sky densities varying from 10deg^{-2} to 280deg^{-2} as shown. The assumed QSO correlation function amplitude was $s_0 = 6h^{-1}\text{Mpc}$. Also shown is the effective volume for the BOSS LRG survey at $z \approx 0.5$ assuming $s_0 = 10h^{-1}\text{Mpc}$ and 10000deg^2 area. The WiggleZ ELG survey at $z \approx 0.5$ has $s_0 = 4.4h^{-1}\text{Mpc}$ and 1000deg^2 area. The proposed BigBOSS ELG survey at $z \approx 1$ has $s_0 = 4.4h^{-1}\text{Mpc}$ and 14000deg^2 area. The arrows indicate the positions of the 1st, 2nd, 3rd and 4th BAO peaks (from left to right).

The main change from the previous 2QZ mocks is that the QSO sky density is approximately doubled from 35deg^{-2} to 75deg^{-2} . The area of the mock survey is $15 \times 75\text{deg}^2$ or $1.5 \times$ the area of the 2QZ survey. Previously we have shown that our correlation function and power-spectrum estimation techniques can accurately retrieve the input functions in real and redshift space. The errors are jack-knife estimates based on 60 sub-samples from this contiguous area. The amplitude of the correlation function at small scales is $r_0 = 6h^{-1}\text{Mpc}$, close to the $r_0 = 5.9h^{-1}\text{Mpc}$ shown by the data.

Fig. 3 shows the large-scale correlation functions from the mocks with 1125deg^2 area and 80 and 280deg^{-2} QSO sky densities. We find that the errors are compatible with those extrapolated using simple Poisson scaling of the data-data pairs from the 2QZ+2SLAQ survey with its smaller QSO sky density and area. In fact, we find that in the relatively small area of the Hubble Volume simulation the BAO peak is barely detected, in either the mock at the standard QSO sky density of 80deg^{-2} or even at 280deg^{-2} . In the $\xi(s)$ measured for the unbiased mass (not shown), the feature is detected but only at low significance, $1-2\sigma$. Thus although no feature is detectable in the relatively small Hubble Volume mocks, these data can still be used to estimate the likely errors in the $\approx 3 \times$ bigger 3000deg^2 nominal QSO survey considered in Section 3 above.

Fig. 4 shows the ratio of the jack-knife errors (60 sub-samples) from the above QSO mock catalogues from the Hubble Volume simulations. The ratio of the errors agrees with the Poisson prediction between the 35deg^{-2} and 80deg^{-2} (also 105deg^{-2} see later) sky densities but the in-

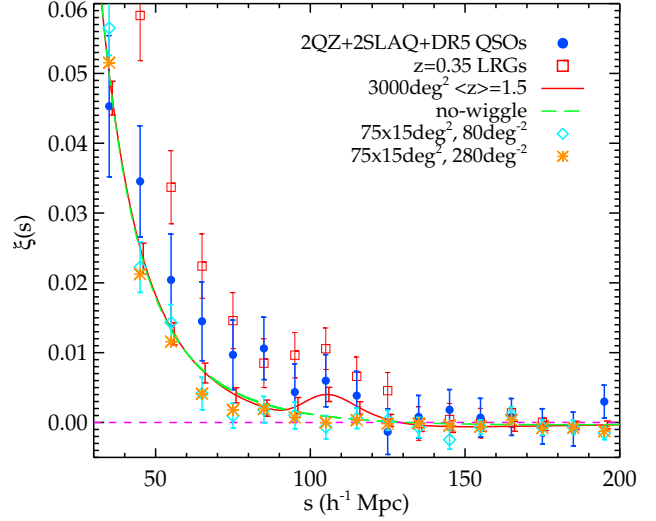


Figure 3. Correlation function from QSO Hubble Volume mocks at 35 , 80 and 280deg^{-2} compared to ΛCDM and no-wiggle models and also the observed data. The errors found for the 80deg^{-2} case have been scaled to a 3000deg^2 survey and applied to the ΛCDM model (red points + line).

crease to 140deg^{-2} and 280deg^{-2} only achieves a factor of 3.3 and 5 improvement in the error rather than the Poisson predicted factor of 4 and 8 , respectively. So Poisson scaling works as far as the sky density of $\approx 100\text{deg}^{-2}$.

4.2 Log-normal simulations

We also ran static simulations similar to the Gaussian simulations of Blake & Glazebrook (2003); Glazebrook & Blake (2005), drawing 3-D mode amplitudes according to power spectra for a standard ΛCDM model. The distribution used for these realisations was up-dated to log-normal rather than Gaussian to mimic better the effects of non-linearities in the matter distribution (Coles & Jones 1991; Blake et al. 2011). Fig. 5a shows the $P(k)$ analysis of 400 simulations for a 3000deg^2 , $z < 2.2$ QSO survey with sky density 90deg^{-2} and a uniform space density of $n = 1.6 \times 10^{-5}\text{h}^3\text{Mpc}^{-3}$. We split the redshift range into 3 parts, $0.4 < z < 1.0$, $1.0 < z < 1.6$ and $1.6 < z < 2.2$ with QSO sky densities of 18 , 33 and 39deg^{-2} with an infall parameter of $\beta = 0.58, 0.43, 0.32$ and $b = 1.4, 2.1, 3.0$ in successive redshift ranges (Croom et al. 2005). Although the sample is dominated by shot noise, BAOs are detectable in $P(k)$ in the 2nd and 3rd slices with a precision comparable to WiggleZ and SDSS-LRGs. In Fig. 5a, the dotted lines are the result of an effective volume calculation for the errors, which agrees well with the scatter in the lognormal realizations. The accuracy in the $P(k)$ BAO comes from fitting the simple Blake & Glazebrook (2003); Blake et al. (2006) model to the realizations. We detect the BAO in the $1 < z < 1.6$ bin with $\pm 5\%$ accuracy for the BAO scale and in the $1.6 < z < 2.2$ bin with $\pm 3.7\%$ accuracy. Overall the BAO scale accuracy in the $1 < z < 2.2$ range and $\approx 70\text{deg}^{-2}$ sky density is $\pm 3\%$.

Fig. 5b shows the mean correlation function result integrated over the full $0.4 < z < 2.2$ redshift range. Again we see the BAO feature clearly detected at $\approx 3\sigma$ relative to zero signal.

5 QSO DARK ENERGY SURVEY

5.1 Empirical survey parameter estimates

We first take the empirical, jack-knife error estimates at $100h^{-1}\text{Mpc}$ from the 2QZ $\xi(s)$ result, also shown in Fig. 1. Ignoring the 2SLAQ survey simplifies the scaling of errors since in the Northern Cap at least, 2SLAQ relied on 2QZ to supply the QSOs with $b_J < 20.85$. We can then simply scale the errors from 2QZ assuming a sky density of 35deg^{-2} and an area of 750deg^2 . The 2QZ amplitude and error in Fig. 1 suggest that a BAO peak at $\approx 100h^{-1}\text{Mpc}$ will appear at the $\approx 1\sigma$ level in a QSO sample of the current size (0.86σ against the no-wiggle-model and 1.1σ against zero correlation signal). Hence a $\approx 4\sigma$ detection will require either a $16\times$ bigger survey at the 35deg^{-2} density or a $4\times$ bigger survey at double the QSO sky density. The simulation results in Fig. 4 suggest that this Poisson sky density scaling continues at least as far as $\approx 100\text{deg}^{-2}$ but not as far as 280deg^{-2} . Fig. 2 also suggests that the error is $3\times$ rather than $4\times$ smaller at a QSO sky density of 140deg^{-2} compared to 35deg^{-2} , so a survey of only $\approx 1300\text{deg}^2$ would be required to achieve a 4σ BAO detection. By mainly using previous 2QZ and 2SLAQ survey areas and taking tiling overlaps of $\approx 20\%$ into account (to ensure survey areal completeness), the sky density for new QSO targets might only be $\approx 100\text{deg}^{-2}$, or ≈ 300 per 2dF field. If these QSOs could be efficiently detected with a contamination of only 25% or less then it may be possible to achieve this density with only a single 2dF pointing per field. 2SLAQ achieved a 44% star contamination rate based on SDSS single epoch imaging data and improving on this rate mostly depends on achieving improved *ugriz* photometry compared to SDSS. This should be possible using new surveys such as VST ATLAS (Shanks et al. 2011, in prep.). Note also that 2SLAQ used more traditional colour cuts, and methods such as KDE (e.g. Richards et al. 2009), extreme-deconvolution etc., would improve target selection considerably.

5.2 Simulated survey parameter estimates

We then take the jack-knife based error estimates from the Hubble Volume simulation. As noted above, we have checked that the jack-knife errors reduce approximately linearly as the QSO density increases up to $\approx 80\text{deg}^{-2}$. Fig. 4 shows that as the mock QSO sky density rose from 35 to 80, 140 and then 280deg^{-2} , factors of 2.3, 4 and 8.0, the jack-knife error in 60 subsamples reduced by factors of 2.22 ± 0.28 , 3.34 ± 0.31 and 5.0 ± 0.64 . If we drop the $z < 1$ QSOs (see below) in the 140deg^{-2} mock catalogue, the sky density becomes 105deg^{-2} and the error on the $\xi(s)$ only increases by 10%. Care was taken here that the small scale correlation function amplitude remained constant at the three sky densities so that the effect of sky density could be easily measured. These ratios also reasonably agree with taking ratios of the average of the square root of the three lowest k effective volumes in Fig. 2. So we again conclude that at least up to a sky density of $\approx 100\text{deg}^{-2}$, doubling the sampling rate approximately halves the error. We also see that for the 80deg^{-2} QSO mock, extrapolating the error from the mock survey area of 1125deg^2 to 3000deg^2 , indicates that the error is reduced to $\approx 27\%$ of the error in the 2QZ $\xi(s)$

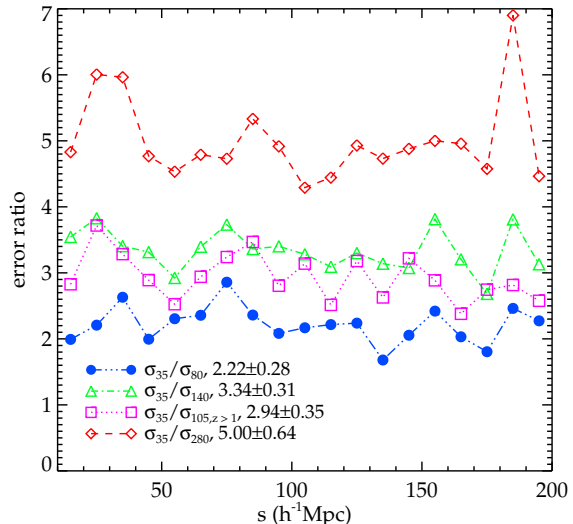


Figure 4. The ratio of the jack-knife errors (60 sub-samples) from the QSO mock catalogues from the Hubble Volume N-Body simulation, using densities of 35deg^{-2} , 80deg^{-2} , 140deg^{-2} and 280deg^{-2} . The final ratios of 2.22 ± 0.28 , 2.94 ± 0.35 , 3.34 ± 0.31 and 5.0 ± 0.64 can be compared to the QSO sky density ratios of 2.29, 3.0, 4.0 and 8.0, confirming that the error scales as expected from Poisson statistics between 35 and $\approx 100\text{deg}^{-2}$.

results of Fig. 1, again indicating that these survey parameters will produce an $\approx 4\sigma$ detection of the BAO feature in $\xi(s)$. Finally, the error on the $\xi(s)$ peak at $\approx 105h^{-1}\text{Mpc}$ in the log-normal simulations in Fig. 5b represents again an $\approx 3-4\sigma$ detection. So there is generally excellent agreement between simulated estimates and the empirical results from Section 5.1 that a 3000deg^2 QSO survey with an $80-90\text{deg}^{-2}$ QSO sky density will produce a significant detection of the BAO peak with a scale measurable to $\approx \pm 3\%$.

5.3 Comparison with other surveys

Fig. 6 compares the combined $1 < z < 2.2$ BAO error for the dilation scale, $D_V(z) = (D_A(z)^2 cz/H(z))^{1/3}$, of a nominal 3000deg^2 , 90deg^{-2} QSO survey with other current BAO surveys. The dilation scale is a measure which combines the information in the comoving angular diameter distance, $D_A(z)$, and the Hubble parameter, $H(z)$. The errors are now generated using the fitting formula of Blake et al. (2006) which is calibrated by lognormal realizations (Glazebrook & Blake 2005) for the BAO measurements. We see that the $\approx \pm 4\%$ error from the QSO survey is comparable to the BAO error at $z = 0.35$ from the SDSS LRG survey and WiggleZ at $z = 0.6$. Note that the error derived for the dilation scale from the QSO survey-specific log-normal simulations described above is $\pm 3\%$ which is clearly the more directly measured result. The results in Fig. 6, on the other hand, have the advantage that they are measured consistently between the various surveys.

In response to a request from a referee, we note that the Hobby-Eberly Telescope Dark Energy Experiment HETDEX survey (Hill et al. 2008) will allow ≈ 750000 Ly- α emitting galaxies to be mapped over $1.9 < z < 3.5$ in

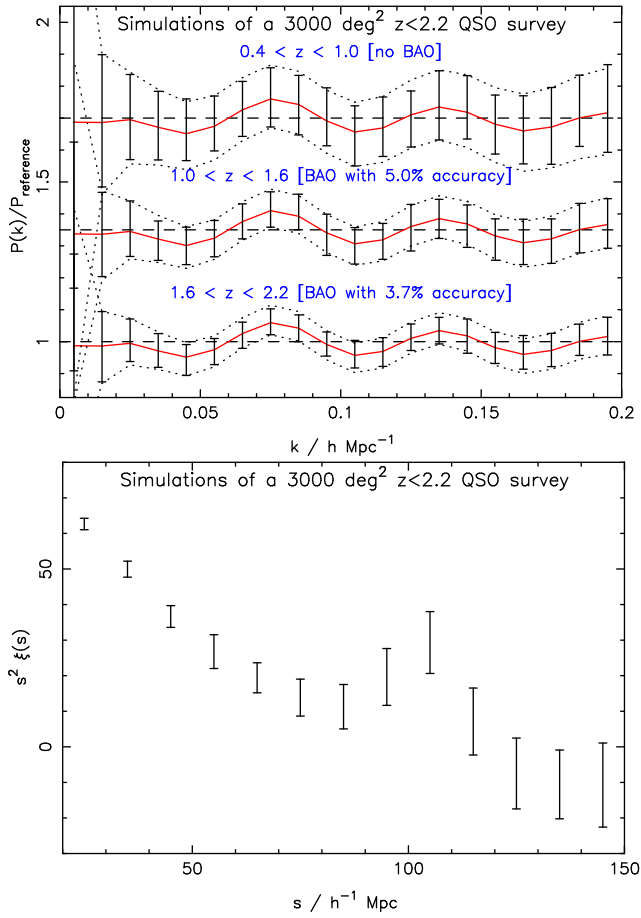


Figure 5. (a) Predicted survey sensitivity for BAO from 400 log-normal simulations. Each successive set of data has been offset in y for clarity. QSO Power-spectrum BAO accuracy is 3% over full $1 < z < 2.2$ range in nominal survey. (b) The QSO $\xi(s)$ from the log-normal simulations integrated over the $0.4 < z < 2.2$ redshift range. The BAO signal is clearly detected.

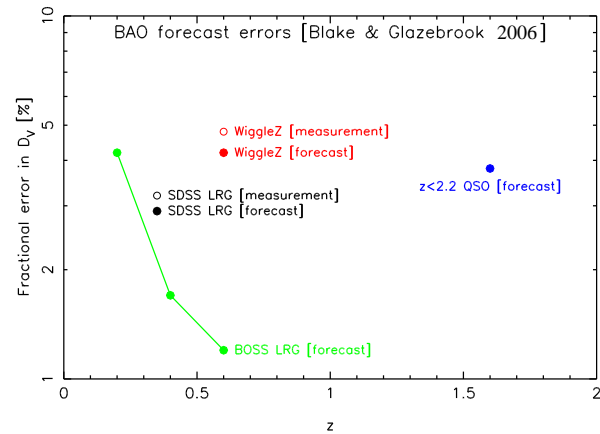


Figure 6. Predicted sensitivity for BAO in the nominal QSO survey consistently compared with other surveys. QSO power spectrum BAO accuracy forecasts from the fitting formula of Blake et al. (2006).

420deg^2 of sky in 150 clear nights. This survey is claimed to measure the BAO scale to $\approx 1\%$ accuracy. This survey will therefore produce similar errors to a QSO survey with an area of 4500deg^2 and a sky density of $\approx 100\text{deg}^{-2}$, in a mostly higher and hence complementary redshift range.

5.4 Markov Chain Monte Carlo cosmology fits

Finally, we ran some MCMC cosmology fits for WMAP distance priors plus current and future BAO surveys for $(\Omega_m, \Omega_m h^2, w_0, w_a, \Omega_k)$ with the motivation of seeing if the data can distinguish curvature from evolving dark energy. For that reason we first focus on the joint likelihood of (w_a, Ω_k) , which is shown in Fig. 7a for various combinations of surveys. We assume the CPL (Chevallier & Polarski 2001; Linder 2003) parameterisation for the evolving dark energy equation of state, i.e. $w(a) = w_0 + w_a(1-a)$. For the WMAP distance data we used the constraints on the shift parameter R , the acoustic scale l_a and the redshift of recombination z_* , as given in Komatsu et al. (2009).

Given just SDSS-LRG + WiggleZ (not shown), our nominal $3000\text{deg}^2/80\text{deg}^2$ QSO survey at $z = 1.6$ does give significant help. However, Fig. 7a is based on WMAP +BOSS-LRG (+BOSS-Ly α) and the accuracy of particularly the BOSS-LRG measurement at $z \approx 0.5$ provided by this combination means that the QSOs (green contour) will only decrease the errors in w_a, Ω_k by at most 10-20% in this parameterization. Clearly in the case where there is little evolution and $w_a \approx 0$, even in their more restricted redshift ranges, BOSS LRG and Ly- α surveys already constrain w_a as strongly as the nominal $3000\text{deg}^2 + 80\text{deg}^{-2}$ QSO survey at $z \approx 1.6$. The same result holds in the w_0, w_a plane in Fig. 7b. *On the other hand, it should be noted that the nominal QSO survey would on its own produce the first detection of, for example, discontinuous dark energy evolution in the so far unexplored $1 < z < 2.2$ redshift range.*

We next consider what survey parameters would lead to significant improvements in the cosmological forecasts, even in the case where the dark energy evolves smoothly from $z \approx 0.5$ to $z \approx 1.6$. Bigger QSO surveys shown in Fig. 7a,b assume 1% and 2% errors in D_V and the contours suggest that a 1.5% error is likely to give significantly smaller errors than the competing BOSS LRG+Lyman- α surveys in the w_a, Ω_k and the w_0, w_a planes.

If so, then we would need to increase the QSO sky density by a factor of ≈ 1.6 to $\approx 140\text{deg}^{-2}$, reducing the QSO D_V error by a factor of ≈ 1.5 from 3% to 2%. This would require a 0.6mag fainter mag limit taking us to $g < 22.5$ rather than $g < 21.85$. Then we could drop the $z < 1$ QSOs which takes us back to $\approx 105\text{deg}^{-2}$ (see Section 5.2), without much loss of BAO S/N as evidenced from the log-normal simulations and Fig. 4. This should be possible with VST ATLAS imaging data. If we wanted to get below a 2% error then an additional $\approx 50\%$ of the area ie $\approx 4500\text{deg}^2$ would give a BAO error of 1.6%. This may be possible in a 1-2hr AAOmega exposure time and the survey would then be completed in ≈ 200 clear nights. From Figs. 7, such a QSO survey would produce an error on the dark energy evolution parameter, w_a , which is $\approx 60\%$ the size of that from BOSS LRGs. The BAO detection significance would be $\approx 6\sigma$ as opposed to $3 - 4\sigma$ in the nominal $3000\text{deg}^2, 80\text{deg}^{-2}$ QSO survey.

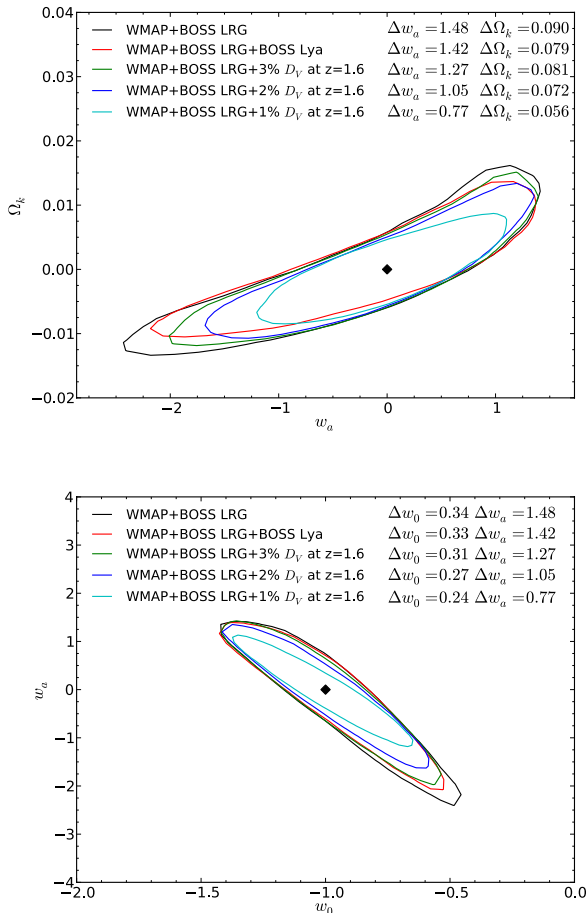


Figure 7. Predicted survey constraints for Ω_k , w_a , w_0 from BAO MCMC fits. 1σ contours and errors are shown. **(a)** Our nominal QSO survey produces a 3% BAO error (green contour) and will provide the first detection of any non-standard (eg discontinuous) evolution in the dark energy equation of state in the $1 < z < 2$ range. But if the evolution remains relatively standard/continuous then a survey with a 50% bigger area and a 50% higher sky density will produce a 1-2% QSO BAO error which will significantly improve over BOSS constraints on w_a and Ω_k (cyan, blue contours). **(b)** Similarly, even in the case of standard/continuous dark energy evolution, a survey with a 1-2% BAO error will provide significantly improved constraints over BOSS in the (w_0, w_a) plane (cyan, blue contours).

5.5 Redshift-space distortions

The nominal 3000deg^2 redshift survey of 250000 QSOs would also be able to probe cosmology via redshift-space distortions. Now a redshift-space distortion test of non-Einstein gravity is more difficult at high redshift because $\Omega_m(z)$, at least in FLRW-based models, tends to unity at high z , making the γ index of the gravitational growth rate (Linder 2005), $f(z) = \Omega_m(z)^\gamma$, more difficult to determine. However, interesting cosmological constraints can still be obtained. The infall parameter governing redshift-space distortions, is defined as $\beta = \Omega_m^\gamma/b$, and so depends on the bias, b , as well as the gravitational growth rate, Ω_m^γ . Previously for the 2QZ and 2SLAQ QSO surveys we have used redshift-space distortion and the evolution of the QSO clustering amplitude

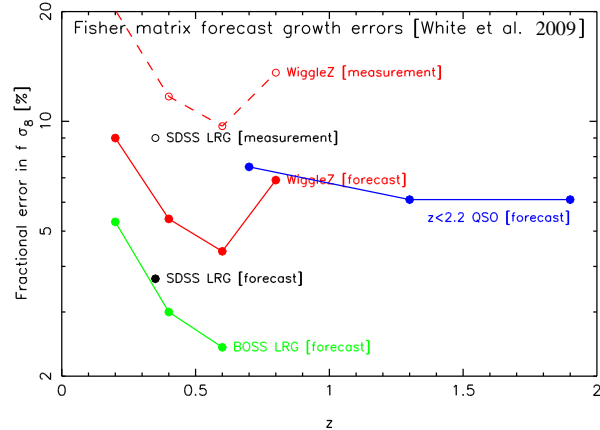


Figure 8. Predicted sensitivity for growth of structure in the nominal QSO survey consistently compared with other surveys. Growth of structure forecasts are generated using the Fisher matrix formula of White, Song, & Percival (2009).

to solve for $\Omega_m(z=0)$ and bias, $b(z=1.6)$ simultaneously (da Ângela et al. 2005; da Ângela, Outram, & Shanks 2005; da Ângela et al. 2008). This test also involves the Alcock-Paczynski geometric test. The bias, $b(z=1.6)$ can then be used to derive the amplitude of mass clustering, ie σ_8 , at $z=1.4$.

Recently, the combination $f \times \sigma_8^m$ ($= \beta \times \sigma_8^g$ if $b = \sigma_8^g/\sigma_8^m$) has become the prime target for redshift-space distortion studies, since it can discriminate between modified gravity models without needing to determine the bias (Song & Percival 2009). Redshift space distortions can thus provide a strong test of Einstein's gravity independently of geometrical cosmological tests that use standard candles and rods, such as BAO (Guzzo et al. 2008). Redshift-space distortions can further be used to give an estimate of the masses and hence mass-to-light ratios of galaxy group haloes in CDM models (e.g. Mountrichas et al. 2009).

In Fig. 8, we show the error in the gravitational growth rate - mass fluctuation parameter, $f\sigma_8$, for the QSO survey as estimated using the publicly available Fisher matrix code of White, Song, & Percival (2009). The result is averaged over the full range of clustering scales $1 < s < 100h^{-1}\text{Mpc}$. We see that the overall result is again comparable to that for WiggleZ (Blake et al. 2011) and the SDSS LRG survey but at a significantly higher redshift. If we made a survey at the $\approx 140\text{deg}^{-2}$ QSO density and over an area of 4500deg^2 , the error on these redshift space distortion results would reduce by a further factor of $\approx 1.8\times$. So with these parameters the error on $f\sigma_8$ would reduce from 6% to 3.3% in this redshift range making the survey even more competitive in the $1 < z < 2.2$ range.

6 QSO CLUSTERING AS A PROBE OF NON-GAUSSIANITY

6.1 Background

Inflationary models with standard slow-roll inflation will produce very little non-Gaussianity, but models that deviate from the slow-roll assumption can produce a sig-

nificantly non-Gaussian seed field (see Bartolo et al. 2004 for a review). Non-Gaussianity is normally parameterised through some amplitude of a quadratic term in the primordial Bardeen potential, f_{NL} . This parameter gives the coupling between a triangle of three k -modes, and can either be applied to the local ('squeezed' isosceles triangles) or equilateral form of non-Gaussianity. It can be measured using the large scale galaxy Bispectrum. The best current limits on non-Gaussianity are obtained from the cosmic microwave background radiation (CMB; Komatsu et al. 2011) who found $f_{NL}^{local} = 32 \pm 21$. Galaxy surveys can actually be more powerful as they can sample more modes in 3-D space than the CMB can on the 2-D surface of the sphere. It also samples the structure of matter perturbations at smaller scales, making it complementary to experiments such as Planck. By probing scales in the range $k = 0.01 - 0.2 h\text{Mpc}^{-1}$, it will be able to link constraints from the CMB with constraints from clusters (LoVerde et al. 2008), constraining possible scale-dependence of the non-Gaussianity.

In galaxy surveys, non-Gaussianity can produce a scale-dependent boost of the halo power-spectrum at $k < 0.03 h\text{Mpc}^{-1}$ and this evolves as $(1+z)$. Although this can potentially be confused with the full general relativistic correction of the galaxy power spectrum at $k \leq 0.01 h\text{Mpc}^{-1}$, the effect becomes important only beyond $z \approx 3$ (Yoo 2010). Hence QSO surveys with their large volumes and redshift ranges make an ideal basis for this test (e.g. Slosar et al. 2008). Xia et al. (2010a,b) has recently produced upper limits on non-Gaussianity from the SDSS-DR6 photo- z QSO catalogue (Richards et al. 2009) and The NRAO VLA Sky Survey (NVSS; Condon et al. 1998). The NVSS auto-correlation function shows some evidence for a positive tail extending to 5-6 degrees (Xia et al. 2010a, confirming previous results from Blake & Wall 2002) which could be caused by non-Gaussianity, implying $f_{NL}^{local} = 62 \pm 27$. Xia et al. (2010b) found lower but still consistent angular correlation functions from a million QSOs in the SDSS DR6 dataset, implying $f_{NL}^{local} = 58 \pm 24$. However, f_{NL} measurements from high- z photometric surveys can contain systematic bias due to gravitational lensing magnification (Namikawa et al. 2011). QSO redshift surveys will provide more accurate and stringent constraints.

6.2 Non-Gaussianity constraints via the nominal QSO survey

A 3000deg^2 QSO survey will give highly competitive constraints on primordial non-Gaussianity in the density field. Sefusatti & Komatsu (2007) calculated how effective future galaxy surveys would be at measuring the f_{NL} parameters, simultaneously with the non-linear bias. Their Fig. 6 shows predictions of the sensitivity of surveys of different volumes with a galaxy density of $5 \times 10^{-4} (\text{h}/\text{Mpc})^3$. Their forecasts demonstrate that our nominal QSO survey has certain advantages over its low redshift counterparts. By making measurements at higher redshift, it is less affected by non-linear structure formation, and can measure the Bispectrum down to smaller scales. Its main advantage will be its volume, which will be larger than most other funded surveys planned for $z > 1$. We estimate that our survey will be able to constrain f_{NL} (local) with an error of about

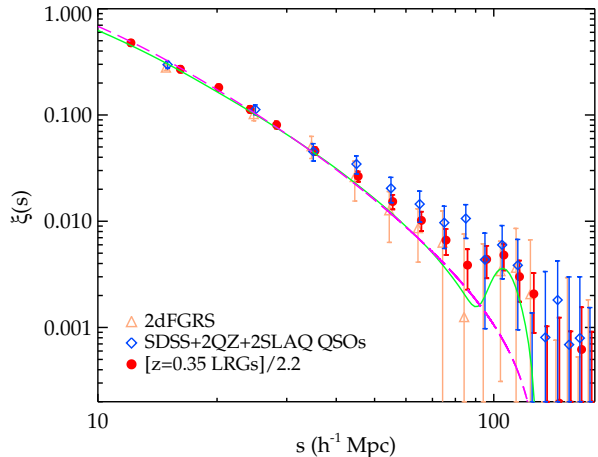


Figure 9. The combined DR5+2QZ+2SLAQ QSO correlation function from Figs. 1 now plotted on log axes and compared to the 2dFGRS $\xi(s)$ at $z \approx 0.12$ of Hawkins et al and the scaled SDSS LRG $\xi(s)$ of Eisenstein et al and a linear model fitted to LRG surveys in the range $0.35 < z < 0.7$. The slope of the QSO $\xi(s)$ at $z \approx 1.6$ is marginally (2σ) flatter than the linear model fitted at $z < 0.7$.

± 15 , and f_{NL} (equilateral) of about ± 150 , according to the Sefusatti & Komatsu (2007) analysis. This is better than any current survey : these authors predict uncertainties almost $10\times$ larger for the SDSS-LRG survey, for example. Our estimate is similar to the best current CMB result, but this would be the first competitive test made using QSOs.

6.3 Testing for non-Gaussianity via large-scale clustering evolution

Recently, angular correlation function studies of EROs in SA22 at $z \approx 1.5$ (Kim et al. 2011) and LRGs in SDSS Stripe 82 at $z \approx 1$ (Nikoloudakis et al. 2011) have shown evidence for a flatter slope in the range $10 < r < 100 h^{-1}\text{Mpc}$ compared to the lower redshift, SDSS ($z \approx 0.35$), 2SLAQ ($z \approx 0.55$) and AAOmega LRG ($z \approx 0.68$) surveys. The evolution is small but statistically reasonably significant ($\approx 3\sigma$). Since evolution is not expected in the linear regime in the standard cosmological model, one interpretation of this evolution is that it might correspond to evidence for a non-Gaussian feature in the galaxy correlation function becoming more prominent at high redshifts, similar to that found above by Xia et al. (2010a); Blake & Wall (2002).

However, the angular correlation function is particularly susceptible to artefacts in the data such as small artificial gradients. The amplitude of the redshift space correlation function is intrinsically higher because of the lack of projection effects. Therefore it is interesting to use the QSO clustering correlation function, $\xi(s)$, to look for evolution in the large-scale slope of the correlation function. In Fig. 9 we therefore compare the combined QSO correlation function to the 2dFGRS $\xi(s)$ at $z \approx 0.12$ (Hawkins et al. 2003) and the SDSS LRG $\xi(s)$ at $z \approx 0.35$ (Eisenstein et al. 2005). We also show a linear model that was fitted to correlation functions from 1.5 million LRGs in three photometric samples with average redshifts $z = 0.35, 0.55, 0.68$ (Sawangwit et al. 2011). This

model assumes a Λ CDM Universe with $\Omega_\Lambda = 0.73$, $\Omega_m = 0.27$, $f_{\text{baryon}} = 0.167$, $\sigma_8 = 0.8$, $h = 0.7$ and $n_s = 0.95$. This model has also been corrected for scale-dependent redshift-space distortion following Eisenstein et al. (2005). It can be seen that this model also gives an excellent fit to the 2dFGRS ($z = 0.12$) and SDSS LRG ($z = 0.35$) 3-D correlation functions, $\xi(s)$, as shown. At the level of the current errors in the observed correlation functions, it is not possible statistically to distinguish the form of the observed low- z galaxy and high- z QSO correlation functions. However, when χ^2 fitted in the $15 < s < 95h^{-1}\text{Mpc}$ range, the slope of the $z \approx 1.6$ QSO correlation function appears flatter at the 2σ level than the linear model fitted to the lower redshift ($z < 0.7$) surveys.² This provides some limited support to the results from the LRG angular correlation functions at $z = 1$ and $z = 1.5$ but clearly more data are needed. Even the nominal QSO survey would provide an $\approx 3 - 4\times$ reduction in the errors in the $10\text{-}100h^{-1}\text{Mpc}$ range and allow a much more significant search for non-Gaussian evolution at large QSO separations. Furthermore, the possible detection of non-Gaussian evolution in the current LRG and QSO surveys is a potent reminder that dark energy evolution at high redshift may also be of an unexpected form which should be measured rather than assumed.

7 OTHER QSO Z SURVEY SCIENCE

More QSOs will also provide new data on the small-scale amplitudes of QSO clustering as a function of luminosity and will improve $\xi(s)$ statistics at SDSS, 2QZ and 2SLAQ depths and this has importance for QSO formation and evolution models. The amplitude of QSO clustering seems remarkably independent of QSO luminosity (Shanks et al. 2011), is marginally significant (Porciani & Norberg 2006 and Shen et al. 2009), and so checking for any small luminosity dependence can put strict limits on models of QSO environment and their host halo and BH mass. A 3000deg^2 survey will contain 30000 QSOs at the SDSS depth, ≈ 100000 at the 2QZ flux limit and ≈ 120000 at the 2SLAQ limit, so there will be significant improvements in the small-scale QSO clustering measurements in all 3 luminosity ranges.

A further application of a QSO survey is QSO lensing via magnification bias (Myers et al. 2003, 2005; Scranton et al. 2005; Ménard et al. 2010). Myers et al found stronger results using QSO spectroscopic z than Ménard et al did using QSO photo- z . Mountrichas & Shanks (2007) found that contamination of the photo- z QSO sample by low redshift QSOs could reduce the anti-correlation signal that is expected from lensing of faint QSOs. A large spectroscopic QSO survey would reduce the errors on the 2QZ results significantly and test the validity of the photo- z results, as well as complementing galaxy shear weak-lensing tomography.

QSO surveys also allow investigations of the topology of the Universe. For example, using the 2QZ survey, Weatherley et al. (2003) searched for exact QSO spectral pairs at large separations to check for topologically closed

universes. Again a larger QSO survey would allow more stringent constraints on such models.

8 SUMMARY AND CONCLUSIONS

We first made a new correlation function analysis of the combined SDSS, 2QZ and 2SLAQ QSO surveys, comprising some 60000 QSOs. We focussed on the large-scale, $s \approx 100h^{-1}\text{Mpc}$, results to test the strength of BAO signal that could be detected in the current dataset. We found that the ≈ 22000 2QZ QSOs dominate the signal; although 2SLAQ has a higher sky density it has only ≈ 6000 QSOs in total and although SDSS has a larger number of QSOs its contribution is less significant because of its low sky density. We observe a possible peak at $\approx 105h^{-1}\text{Mpc}$ where the SDSS LRG $\xi(s)$ peak was found by Eisenstein et al. (2005) but here it is only detected at a low significance of $\approx 1\sigma$ in the combined dataset and other peaks are seen at other separations at a similar significance.

We then proceeded to investigate the QSO survey parameters that would be needed to make an $\approx 4\sigma$ detection of the BAO peak. We conclude that our nominal survey of 250000 QSOs in a sky area of 3000deg^2 will allow us to make a 4σ detection of the BAO scale at $1 < z < 2.2$, an as yet unexplored range for cosmology. This $\pm 3\%$ BAO scale measurement will determine the high-redshift evolution of the dark energy equation of state, $p = w(z)\rho$, and in particular show if there is any large ($> 15\%$) deviation from $w = -1$ in the $1 < z < 2.2$ redshift range. But even if $w_a \approx 0$, then a survey with 50% higher QSO sky density and a 50% bigger area will approximately halve the BAO error to 1.6%. At this point the QSO survey will also approximately halve the error on the dark energy evolution parameter, w_a , and significantly reduce the errors on w_0 and Ω_k compared to the BOSS LRG and Lyman- α BAO results at lower and higher redshifts.

A QSO survey can also set powerful new limits on the existence of non-Gaussianity (f_{NL}) in the primordial density field. We have found that the combined SDSS+2QZ+2SLAQ QSO survey shows possible $\approx 2\sigma$ evidence for evolution in the linear form of the $z \approx 1.6$ QSO correlation function, in the sense that it shows a flatter slope than a linear model fitted to galaxy surveys at $z < 0.7$. Even the nominal QSO survey would improve the significance of detection of this slope change by $3 - 4\times$. If confirmed, the result could indicate the detection of the evolution of a non-Gaussian feature in the large-scale QSO correlation function. The tentative evidence found here and in projected galaxy correlation functions for unexpected evolution of large-scale structure emphasises that dark energy evolution at high redshift may also be of an unexpected form.

The QSO survey will further support analyses of redshift space distortions to measure $f \times \sigma_8$ and test Einstein gravity versus other modified gravity models. We shall also make the most rigorous application of the Alcock & Paczynski (1979) test so far of the prediction of the standard Λ CDM model for the amplitude of the mass clustering, σ_8 , at $z \approx 1.5$. Other science it will do includes making the most accurate determination of the luminosity dependence of QSO clustering at small scales in order to probe QSO formation and evolution via QSO environment.

² Since the jack-knife errors are approximately Poisson in this range, we have ignored the covariance between points in our χ^2 analysis.

The survey could also use QSO lensing magnification bias to measure the mass and the bias of foreground groups and clusters and to do lensing tomography.

ACKNOWLEDGMENTS

We acknowledge Chris Blake for allowing us to access the results from log-normal simulations of Blake & Glazebrook (2003); Blake et al. (2006) and publicly available Fisher matrix codes. We thank the referee for useful comments which helped improve the paper.

US acknowledges financial support from the Institute for the Promotion of Teaching Science and Technology (IPST) of The Royal Thai Government.

We thank all the present and former staff of the Anglo-Australian Observatory for their work in building and operating the 2dF facility.

Funding for the SDSS and SDSS-II has been provided by the Alfred P. Sloan Foundation, the Participating Institutions, the National Science Foundation, the U.S. Department of Energy, the National Aeronautics and Space Administration, the Japanese Monbukagakusho, the Max Planck Society, and the Higher Education Funding Council for England. The SDSS Web Site is <http://www.sdss.org/>.

REFERENCES

- Alcock C., Paczynski B., 1979, *Nature*, 281, 358
 Bartolo N., Komatsu E., Matarrese S., Riotto A., 2004, *PhR*, 402, 103
 Blake C., Wall J., 2002, *MNRAS*, 329, L37
 Blake C., Glazebrook K., 2003, *ApJ*, 594, 665
 Blake C., Parkinson D., Bassett B., Glazebrook K., Kunz M., Nichol R. C., 2006, *MNRAS*, 365, 255
 Blake C., et al., 2011, *MNRAS*, 951
 Boyle B. J., Shanks T., Peterson B. A., 1988, *MNRAS*, 235, 935
 Boyle B. J., Griffiths R. E., Shanks T., Stewart G. C., Georgantopoulos I., 1993, *MNRAS*, 260, 49
 Boyle B. J., Shanks T., Croom S. M., Smith R. J., Miller L., Loaring N., Heymans C., 2000, *MNRAS*, 317, 1014
 Chevallier M., Polarski D., 2001, *IJMPD*, 10, 213
 Condon J. J., Cotton W. D., Greisen E. W., Yin Q. F., Perley R. A., Taylor G. B., Broderick, J. J., 1998, *AJ*, 115, 1693
 Croom S. M., Shanks T., 1996, *MNRAS*, 281, 893
 Coles P., Jones B., 1991, *MNRAS*, 248, 1
 Croom S. M., Smith R. J., Boyle B. J., Shanks T., Miller L., Outram P. J., Loaring N. S., 2004, *MNRAS*, 349, 1397
 Croom S. M., et al., 2005, *MNRAS*, 356, 415
 Croom S. M., et al., 2009, *MNRAS*, 399, 1755
 da Ângela J., Outram P. J., Shanks T., Boyle B. J., Croom S. M., Loaring N. S., Miller L., Smith R. J., 2005, *MNRAS*, 360, 1040
 da Ângela J., Outram P. J., Shanks T., 2005, *MNRAS*, 361, 879
 da Ângela J., et al., 2008, *MNRAS*, 383, 565
 Eisenstein D. J., Hu W., 1998, *ApJ*, 496, 605
 Eisenstein D. J., et al., 2005, *ApJ*, 633, 560
 Evrard A. E., et al., 2002, *ApJ*, 573, 7
 Fanidakis, N., et al., 2010, *MNRAS*, in prep.
 Fine S., et al., 2006, *MNRAS*, 373, 613
 Fry J. N., 1996, *ApJ*, 461, L65
 Glazebrook K., Blake C., 2005, *ApJ*, 631, 1
 Guzzo L., et al., 2008, *Natur*, 451, 541
 Hamilton A. J. S., 1993, *ApJ*, 417, 19
 Hatton S., Cole S., 1998, *MNRAS*, 296, 10
 Hawkins E., et al., 2003, *MNRAS*, 346, 78
 Heckman T. M., Kauffmann G., Brinchmann J., Charlot S., Tremonti C., White S. D. M., 2004, *ApJ*, 613, 109
 Hill G. J., et al., 2008, *ASPC*, 399, 115
 Hoyle F., Outram P. J., Shanks T., Boyle B. J., Croom S. M., Smith R. J., 2002, *MNRAS*, 332, 311
 Kim J.-W., Edge A. C., Wake D. A., Stott J. P., 2011, *MNRAS*, 410, 241
 E. Komatsu *et al.*, 2009, *ApJS*, 180, 330
 Komatsu E., et al., 2011, *ApJS*, 192, 18
 Landy S. D., Szalay A. S., 1993, *ApJ*, 412, 64
 Lewis I., et al., 2002, *MNRAS*, 334, 673
 Lidz A., Hopkins P. F., Cox T. J., Hernquist L., Robertson B., 2006, *ApJ*, 641, 41
 Linder E. V., 2003, *PhRvL*, 90, 091301
 Linder E. V., 2005, *PhRvD*, 72, 043529
 LoVerde M., Miller A., Shandera S., Verde L., 2008, *JCAP*, 0804, 014
 M nard B., Scranton R., Fukugita M., Richards G., 2010, *MNRAS*, 405, 1025
 Mountrichas G., Shanks T., 2007, *MNRAS*, 380, 113
 Mountrichas G., Sawangwit U., Shanks T., Croom S. M., Schneider D. P., Myers A. D., Pimbblet K., 2009, *MNRAS*, 394, 2050
 Myers A. D., Outram P. J., Shanks T., Boyle B. J., Croom S. M., Loaring N. S., Miller L., Smith R. J., 2003, *MNRAS*, 342, 467
 Myers A. D., Outram P. J., Shanks T., Boyle B. J., Croom S. M., Loaring N. S., Miller L., Smith R. J., 2005, *MNRAS*, 359, 741
 Namikawa, T., Okamura, T., & Taruya, A. 2011, *Phys. Rev. D*, 83, 123514
 Nikoloudakis N., Shanks T., Croom S. M., Fine S., Sawangwit U., 2011, in preparation
 Osmer P. S., 1981, *ApJ*, 247, 762
 Outram P. J., Hoyle F., Shanks T., Croom S. M., Boyle B. J., Miller L., Smith R. J., Myers A. D., 2003, *MNRAS*, 342, 483
 Porciani C., Norberg P., 2006, *MNRAS*, 371, 1824
 Richards G. T., et al., 2009, *ApJS*, 180, 67
 Ross N. P., et al., 2009, *ApJ*, 697, 1634
 Sawangwit U., Shanks T., Abdalla F. B., Cannon R. D., Croom S. M., Edge A. C., Ross N. P., Wake D. A., 2011, *MNRAS*, in press, arXiv:0912.0511
 Schneider D. P., et al., 2007, *AJ*, 134, 102
 Scranton R., et al., 2005, *ApJ*, 633, 589
 Sefusatti E., Komatsu E., 2007, *PhRvD*, 76, 083004
 Shanks T., Croom S. M., Fine S., Ross N. P., Sawangwit U., 2011, *MNRAS*, in press, arXiv:1105.2547
 Shen Y., et al., 2009, *ApJ*, 697, 1656
 Slosar A., Hirata C., Seljak U., Ho S., Padmanabhan N., 2008, *JCAP*, 08, 031
 Smith G. A., et al., 2004, *SPIE*, 5492, 410
 Song Y.-S., Percival W. J., 2009, *JCAP*, 10, 4
 Wake D. A., et al., 2004, *ApJ*, 610, L85

- Wake D. A., et al., 2006, MNRAS, 372, 537
Wake D. A., et al., 2008, MNRAS, 387, 1045
Wang X., Chen X., Zheng Z., Wu F., Zhang P., Zhao Y.,
2009, MNRAS, 394, 1775
Weatherley S. J., Warren S. J., Croom S. M., Smith R. J.,
Boyle B. J., Shanks T., Miller L., Baltovic M. P., 2003,
MNRAS, 342, L9
White M., Song Y.-S., Percival W. J., 2009, MNRAS, 397,
1348
Xia J.-Q., Viel M., Baccigalupi C., De Zotti G., Matarrese
S., Verde L., 2010a, ApJ, 717, L17
Xia J.-Q., Bonaldi A., Baccigalupi C., De Zotti G., Matar-
rese S., Verde L., Viel M., 2010b, JCAP, 8, 13
Yoo, J. 2010, Phys. Rev. D, 82, 083508